DDM Preprint
Editors: editor1, editor2, editor3, editor4

1. Direct simulation of the motion of settling ellipsoids in Newtonian fluid

T.-W. Pan[1], R. Glowinski[2], D.D. Joseph[3], R. Bai[4]

1. Introduction. In this article we first discuss the generalization of a Lagrange multiplier based fictitious domain method [7, 10] to the simulation of the motion of particles of general shape in a Newtonian fluid. Unlike the cases where the particles are spheres, we attach two points, besides the center of mass, to each particle of general shape and move them according to the rigid-body motion of the particle in order to track this motion. The equations describing the motion of these two points are solved by a distance preserving scheme so that rigidity can be maintained. We then apply it to simulate ellipsoids settling in a narrow channel filled with a Newtonian fluid. In the simulations, when there is only one ellipsoid it turns its broadside orthogonal to the stream as expected; for the two ellipsoid case they interact with each other as observed in experiments.

2. A model problem and fictitious domain formulation for three dimensional particulate flow. To perform the *direct numerical simulation* of the interaction between particles and fluid, we have developed a methodology which is a combination of a distributed Lagrange multiplier based fictitious domain (also called domain embedding) method and operator splitting methods [6, 8, 7, 9, 10], this approach (or closely related ones derived from it) has become the method of choice for other investigators around the world (refs., Baaijens in [2] and Wagner et al. in [21]). In the following we are going to recall the ideas at the basis of the above methodology, but with generalization to the motion of a single particle of general shape in a Newtonian viscous incompressible fluid (of density ρ_f and viscosity ν_f) under the effect of gravity. For the situation depicted in Figure 2.1 below, the flow is modeled by the Navier-Stokes equations, namely, (with obvious notation)

$$\rho_f\Big[\frac{\partial \mathbf{u}}{\partial t} + (\mathbf{u}\cdot\boldsymbol{\nabla})\mathbf{u}\Big] - \nu_f\Delta\mathbf{u} + \boldsymbol{\nabla}p = \rho_f\,\mathbf{g}\ in\ (\Omega\setminus\bar{B})\times(0,T), \tag{2.1}$$

$$\boldsymbol{\nabla}\cdot\mathbf{u} = 0\ in\ (\Omega\setminus\bar{B})\times(0,T). \tag{2.2}$$

$$\mathbf{u}(0) = \mathbf{u}_0(\mathbf{x}), (with\ \boldsymbol{\nabla}\cdot\mathbf{u}_0 = 0) \tag{2.3}$$

$$\mathbf{u} = \mathbf{g}_0\ on\ \Gamma\times(0,T),\ with\ \int_\Gamma \mathbf{g}_0\cdot\mathbf{n}\,d\Gamma = 0, \tag{2.4}$$

where $\Gamma = \partial\Omega$, $\mathbf{g}$ is gravity and $\mathbf{n}$ is the unit normal vector pointing outward to the flow region. We assume a *no-slip condition* on $\gamma(=\partial B)$ The motion of particle B

[1]University of Houston, Department of Mathematics, Houston, Texas 77204, USA, pan@math.uh.edu
[2]University of Houston, Department of Mathematics, Houston, Texas 77204, USA, roland@math.uh.edu
[3]Department of Aerospace Engineering & Mechanics, University of Minnesota, Minneapolis, Minnesota 55455, USA, joseph@aem.umn.edu
[4]Department of Aerospace Engineering & Mechanics, University of Minnesota, Minneapolis, Minnesota 55455, USA, bai@aem.umn.edu

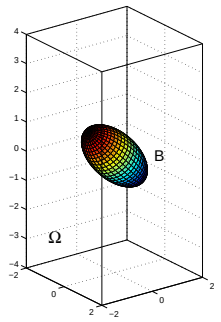

Figure 2.1: The flow region with one particle

satisfies the Euler-Newton's equations, namely

$$\mathbf{v}(\mathbf{x},t) = \mathbf{V}(t) + \boldsymbol{\omega}(t) \times \overrightarrow{\mathbf{G}(t)\mathbf{x}},\ \forall\{\mathbf{x},t\} \in \overline{B(t)} \times (0,T), \tag{2.5}$$

$$\frac{d\mathbf{G}}{dt} = \mathbf{V}, \tag{2.6}$$

$$M_p \frac{d\mathbf{V}}{dt} = M_p\,\mathbf{g} + \mathbf{F}_H + \mathbf{F}^r, \tag{2.7}$$

$$\frac{d(\mathbf{I}_p\,\boldsymbol{\omega})}{dt} = \mathbf{T}_H + \overrightarrow{\mathbf{G}\mathbf{x}_r} \times \mathbf{F}^r, \tag{2.8}$$

with hydrodynamical forces and torques given by

$$\mathbf{F}_H = -\int_\gamma \boldsymbol{\sigma}\mathbf{n}\,d\gamma, \quad \mathbf{T}_H = -(\int_\gamma \overrightarrow{\mathbf{G}\mathbf{x}} \times \boldsymbol{\sigma}\mathbf{n}\,d\gamma), \tag{2.9}$$

completed by the following initial conditions,

$$\mathbf{G}(0) = \mathbf{G}_0,\ \mathbf{V}(0) = \mathbf{V}_0,\ \boldsymbol{\omega}(0) = \boldsymbol{\omega}_0. \tag{2.10}$$

Above, M_p, $\mathbf{I}_p$, $\mathbf{G}$, $\mathbf{V}$ and $\boldsymbol{\omega}$ are the mass, inertia, center of mass, translation velocity of the center of mass and angular velocity of particle B, respectively. In (2.8) we found preferable to deal with the *kinematic angular momentum* $\mathbf{I}_p\,\boldsymbol{\omega}$ making the formulation more conservative. In order to avoid particle-particle and particle-wall penetration which can happen in the numerical simulation, we have introduced an artificial force $\mathbf{F}^r$ in (2.7) (for more details, see, e.g., [7] and [10]) and then a torque in (2.8) acting on the point $\mathbf{x}_r$ where $\mathbf{F}^r$ applies on B.

To solve system (2.1) – (2.10) we can use, for example, *Arbitrary Lagrange-Euler* (*ALE*) methods as in [12, 14, 17], or *fictitious domain methods*, which allow the flow calculation on a fixed grid, as in [6, 8, 7, 9, 10]. The fictitious domain methods that we advocate have some common features with the *immersed boundary method* of Ch. Peskin (see, e.g., refs. [18, 19]) but also some significant differences in the sense that we take systematically advantage of *distributed Lagrange multipliers* to force the rigid body motion inside the particle, which seems still to be a relatively novel approach

in this context, and whose possibilities have not been fully explored yet. As with the methods in [18, 19], our approach takes advantage of the fact that the flow can be computed on a grid which does not have to vary in time, a substantial simplification indeed.

The principle of fictitious domain methods is simple. It consists of

- Filling the particles with a fluid having the same density and viscosity as the surrounding one.
- Compensating the above step by introducing, in some sense, an *anti-particle* of mass $(-1)M_p\,\rho_f/\rho_s$ and inertia $(-1)\mathbf{I}_p\,\rho_f/\rho_s$, taking into account the fact that any rigid body motion $\mathbf{v}(\mathbf{x},t)$ verifies $\boldsymbol{\nabla}\cdot\mathbf{v}=0$ and $\mathbf{D}(\mathbf{v})=\mathbf{0}$ (ρ_s : particle density).
- Finally, imposing the rigid body velocity on $\overline{B(t)}$, namely

$$\mathbf{v}(\mathbf{x},t)=\mathbf{V}(t)+\boldsymbol{\omega}(t)\times\overrightarrow{\mathbf{G}(t)\mathbf{x}},\forall\mathbf{x}\in\overline{B(t)},\forall t\in(0,T), \tag{2.11}$$

  via a Lagrange multiplier $\boldsymbol{\lambda}$ supported by $\overline{B(t)}$. Vector $\boldsymbol{\lambda}$ forces rigidity in $B(t)$ in the same way that $\boldsymbol{\nabla}p$ forces $\boldsymbol{\nabla}\cdot\mathbf{v}=0$ for incompressible fluids.

We obtain then an equivalent formulation of (2.1)–(2.10) defined on the whole domain, namely

For a.e. $t>0$, *find* $\{\mathbf{u}(t),p(t),\mathbf{V}(t),\mathbf{G}(t),\boldsymbol{\omega}(t),\boldsymbol{\lambda}(t)\}$ *such that*

$$\mathbf{u}(t)\in\mathbf{W}_{\mathbf{g}_0}(t),\ p(t)\in L^2_0(\Omega),\ \mathbf{V}(t)\in\mathbb{R}^3,\ \mathbf{G}(t)\in\mathbb{R}^3,\ \boldsymbol{\omega}(t)\in\mathbb{R}^3,\ \boldsymbol{\lambda}(t)\in\Lambda(t) \tag{2.12}$$

and

$$\begin{cases}\rho_f\displaystyle\int_\Omega\left[\frac{\partial\mathbf{u}}{\partial t}+(\mathbf{u}\cdot\boldsymbol{\nabla})\mathbf{u}\right]\cdot\mathbf{v}d\mathbf{x}-\int_\Omega p\boldsymbol{\nabla}\cdot\mathbf{v}d\mathbf{x}+\nu_f\int_\Omega\boldsymbol{\nabla}\mathbf{u}:\boldsymbol{\nabla}\mathbf{v}d\mathbf{x}\\ \quad+(1-\dfrac{\rho_f}{\rho_s})[M_p\dfrac{d\mathbf{V}}{dt}\cdot\mathbf{Y}+\dfrac{d(\mathbf{I}_p\,\boldsymbol{\omega})}{dt}\cdot\boldsymbol{\theta}]-\mathbf{F}^r\cdot\mathbf{Y}-\overrightarrow{\mathbf{G}\mathbf{x}_r}\times\mathbf{F}^r\cdot\boldsymbol{\theta}\\ =<\boldsymbol{\lambda},\mathbf{v}-\mathbf{Y}-\boldsymbol{\theta}\times\overrightarrow{\mathbf{G}\mathbf{x}}>_{\Lambda(t)}+(1-\dfrac{\rho_f}{\rho_s})M_p\ \mathbf{g}\cdot\mathbf{Y}+\rho_f\displaystyle\int_\Omega\mathbf{g}\cdot\mathbf{v}d\mathbf{x},\\ \forall\mathbf{v}\in(H^1_0(\Omega))^3,\ \forall\mathbf{Y}\in\mathbb{R}^3,\ \forall\boldsymbol{\theta}\in\mathbb{R}^3,\end{cases} \tag{2.13}$$

$$\int_\Omega q\boldsymbol{\nabla}\cdot\mathbf{u}(t)d\mathbf{x}=0,\ \forall q\in L^2(\Omega), \tag{2.14}$$

$$\frac{d\mathbf{G}}{dt}=\mathbf{V}, \tag{2.15}$$

$$<\boldsymbol{\mu},\mathbf{u}(t)-\mathbf{V}(t)-\boldsymbol{\omega}(t)\times\overrightarrow{\mathbf{G}(t)\mathbf{x}}>_{\Lambda(t)}=0,\ \forall\boldsymbol{\mu}\in\Lambda(t), \tag{2.16}$$

$$\mathbf{V}(0)=\mathbf{V}_0,\ \boldsymbol{\omega}(0)=\boldsymbol{\omega}_0,\ \mathbf{G}(0)=\mathbf{G}_0, \tag{2.17}$$

$$\mathbf{u}(\mathbf{x},0)=\tilde{\mathbf{u}}_0(\mathbf{x})=\begin{cases}\mathbf{u}_0(\mathbf{x}),\ \forall\mathbf{x}\in\Omega\backslash\overline{B(0)},\\ \mathbf{V}_0+\boldsymbol{\omega}_0\times\overrightarrow{\mathbf{G}_0\mathbf{x}},\ \forall\mathbf{x}\in\overline{B(0)},\end{cases} \tag{2.18}$$

with the following functional spaces

$$\mathbf{W}_{\mathbf{g}_0}(t)=\{\mathbf{v}|\mathbf{v}\in(H^1(\Omega))^3,\ \mathbf{v}=\mathbf{g}_0(t)\ on\ \Gamma\},$$
$$L^2_0(\Omega)=\{q|q\in L^2(\Omega),\ \int_\Omega q\,d\mathbf{x}=0\},\quad \Lambda(t)=(H^1(B(t)))^3.$$

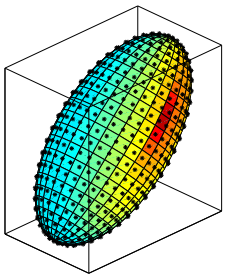

Figure 3.1: An example of grids covering the surface of $B(t)$

In (2.12) – (2.18), only the center of mass, the translation velocity of the center of mass and the angular velocity of the particle are considered. Knowing these two velocities and the center of mass of the particle, one is able to translate and rotate the particle in space by tracking two extra points $\mathbf{x}_1$ and $\mathbf{x}_2$ in each particle, which follow the rigid body motion

$$\frac{d\mathbf{x}_i}{dt} = \mathbf{V}(t) + \boldsymbol{\omega}(t) \times \overrightarrow{\mathbf{G}(t)\mathbf{x}_i}, \quad \mathbf{x}_i(0) = \mathbf{x}_{i,0}, \ i = 1, 2. \tag{2.19}$$

In practice we shall track two orthogonal normalized vectors rigidly attached to the body B and originating from the center of mass $\mathbf{G}$.

3. Time and space discretization. For simplicity, we assume that $\Omega \subset \mathbb{R}^3$ is a rectangular parallelepiped. Concerning the *space approximation* of problem (2.12)–(2.19) by a *finite element method*, we have

$$\mathbf{W}_h = \{\mathbf{v}_h | \mathbf{v}_h \in (C^0(\overline{\Omega}))^3, \ \mathbf{v}_h|_T \in (P_1)^3, \ \forall T \in \mathcal{T}_h\}, \tag{3.1}$$

$$\mathbf{W}_{0h} = \{\mathbf{v}_h | \mathbf{v}_h \in \mathbf{W}_h, \ \mathbf{v}_h = \mathbf{0} \ on \ \Gamma\}, \tag{3.2}$$

$$L^2_h = \{q_h | q_h \in C^0(\overline{\Omega}), \ q_h|_T \in P_1, \ \forall T \in \mathcal{T}_{2h}\}, \quad L^2_{0h} = \{q_h | q_h \in L^2_h, \ \int_\Omega q_h \, d\mathbf{x} = 0\} \tag{3.3}$$

where $\mathcal{T}_h$ is a tetrahedrization of Ω, $\mathcal{T}_{2h}$ is twice coarser than $\mathcal{T}_h$, and P_1 is the space of the polynomials in three variables of degree ≤ 1. A finite dimensional space approximating $\Lambda(t)$ is as follows: let $\{\boldsymbol{\xi}_i\}_{i=1}^N$ be a set of points from $\overline{B(t)}$ which cover $\overline{B(t)}$ (uniformly, for example); we define then

$$\Lambda_h(t) = \{\boldsymbol{\mu}_h | \boldsymbol{\mu}_h = \sum\nolimits_{i=1}^N \boldsymbol{\mu}_i \delta(\mathbf{x} - \boldsymbol{\xi}_i), \ \boldsymbol{\mu}_i \in \mathbb{R}^3, \ \forall i = 1, ..., N\}, \tag{3.4}$$

where $\delta(\cdot)$ is the Dirac measure at $\mathbf{x} = \mathbf{0}$. Then we shall use $< \cdot, \cdot >_h$ defined by

$$< \boldsymbol{\mu}_h, \mathbf{v}_h >_h = \sum\nolimits_{i=1}^N \boldsymbol{\mu}_i \cdot \mathbf{v}_h(\boldsymbol{\xi}_i), \ \forall \boldsymbol{\mu}_h \in \Lambda_h(t), \ \mathbf{v}_h \in \mathbf{W}_h. \tag{3.5}$$

A typical choice of points for defining (3.4) is a collection of grid points for velocity field covered by the interior of the particle $B(t)$ and selected points from the surface of $B(t)$. An example of choice of surface points is shown in Figure 3.1

Using the above finite dimensional spaces leads to the following approximation for problem (2.12)–(2.19):

For a.e. $t > 0$, *find* $\mathbf{u}(t) \in \mathbf{W}_h(t)$, $p_h(t) \in L^2_{0h}(\Omega)$, $\mathbf{V}(t) \in \mathbb{R}^3$, $\mathbf{G}(t) \in \mathbb{R}^3$, $\boldsymbol{\omega}(t) \in \mathbb{R}^3$, $\boldsymbol{\lambda}_h(t) \in \Lambda_h(t)$ *such that*

$$\begin{cases} \rho_f \displaystyle\int_\Omega \left[\frac{\partial \mathbf{u}_h}{\partial t} + (\mathbf{u}_h \cdot \boldsymbol{\nabla})\mathbf{u}_h\right] \cdot \mathbf{v} d\mathbf{x} - \int_\Omega p_h \boldsymbol{\nabla} \cdot \mathbf{v} d\mathbf{x} + \nu_f \int_\Omega \boldsymbol{\nabla}\mathbf{u}_h : \boldsymbol{\nabla}\mathbf{v} d\mathbf{x} \\ \quad +(1 - \frac{\rho_f}{\rho_s})[M_p \frac{d\mathbf{V}}{dt} \cdot \mathbf{Y} + \frac{d(\mathbf{I}_p \boldsymbol{\omega})}{dt} \cdot \boldsymbol{\theta}] - \mathbf{F}^r \cdot \mathbf{Y} - \overrightarrow{\mathbf{G}\mathbf{x}_r} \times \mathbf{F}^r \cdot \boldsymbol{\theta} \\ =< \boldsymbol{\lambda}_h, \mathbf{v} - \mathbf{Y} - \boldsymbol{\theta} \times \overrightarrow{\mathbf{G}\mathbf{x}} >_h + (1 - \frac{\rho_f}{\rho_s}) M_p \mathbf{g} \cdot \mathbf{Y} + \rho_f \displaystyle\int_\Omega \mathbf{g} \cdot \mathbf{v} d\mathbf{x}, \\ \forall \mathbf{v} \in \mathbf{W}_{0h},\ \forall \mathbf{Y} \in \mathbb{R}^3,\ \forall \boldsymbol{\theta} \in \mathbb{R}^3, \end{cases} \tag{3.6}$$

$$\int_\Omega q \boldsymbol{\nabla} \cdot \mathbf{u}_h(t) d\mathbf{x} = 0,\ \forall q \in L^2_h, \tag{3.7}$$

$$\mathbf{u}_h = \mathbf{g}_{0h} \text{ on } \Gamma, \tag{3.8}$$

$$\frac{d\mathbf{G}}{dt} = \mathbf{V}, \tag{3.9}$$

$$\frac{d\mathbf{x}_i}{dt} = \mathbf{V}(t) + \boldsymbol{\omega}(t) \times \overrightarrow{\mathbf{G}(t)\mathbf{x}_i},\ \ \mathbf{x}_i(0) = \mathbf{x}_{i,0},\ i = 1, 2, \tag{3.10}$$

$$< \boldsymbol{\mu}, \mathbf{u}_h(t) - \mathbf{V}(t) - \boldsymbol{\omega}(t) \times \overrightarrow{\mathbf{G}(t)\mathbf{x}} >_h = 0,\ \forall \boldsymbol{\mu} \in \Lambda_h(t), \tag{3.11}$$

$$\mathbf{V}(0) = \mathbf{V}_0,\ \boldsymbol{\omega}(0) = \boldsymbol{\omega}_0,\ \mathbf{G}(0) = \mathbf{G}_0, \tag{3.12}$$

$$\mathbf{u}(\mathbf{x}, 0) = \tilde{\mathbf{u}}_{0h}(\mathbf{x}). \tag{3.13}$$

In (3.8), $\mathbf{g}_{0h}$ is an approximation of $\mathbf{g}_0$ belonging to $\gamma\mathbf{W}_h = \{\mathbf{z}_h | \mathbf{z}_h \in (C^0(\Gamma))^3,\ \mathbf{z}_h = \tilde{\mathbf{z}}_h|_\Gamma \text{ with } \tilde{\mathbf{z}}_h \in \mathbf{W}_h\}$ and verifying $\displaystyle\int_\Gamma \mathbf{g}_{0h} \cdot \mathbf{n} d\Gamma = 0$.

3.1. An operator-splitting scheme à la Marchuk-Yanenko. Many operator-splitting schemes can be used to time-discretize (3.6)–(3.13). One of the advantage of operator-splitting schemes is that we can decouple difficulties like (i) the incompressibility condition, (ii) the nonlinear advection term, and (iii) a rigid-body-motion projection, so that each one of them can be handled separately, and in principle optimally. Let $\triangle t$ be a time discretization step and $t^{n+s} = (n + s)\triangle t$. By an operator-splitting scheme à la Marchuk–Yanenko as in [16], we have the following scheme after dropping some of the subscrips h (similar ones are discussed in [6, 8, 7, 9, 10]):

$$\mathbf{u}^0 = \tilde{\mathbf{u}}_0,\ \mathbf{G}^0 = \mathbf{G}_0,\ \mathbf{V}^0 = \mathbf{V}_0,\ \boldsymbol{\omega}^0 = \boldsymbol{\omega}_0,\ \mathbf{x}_1^0 = \mathbf{x}_{1,0},\ \mathbf{x}_2^0 = \mathbf{x}_{2,0}\ \ \textit{given}; \tag{3.14}$$

for $n \geq 0, \mathbf{u}^n (\simeq \mathbf{u}(t^n))$, $\mathbf{G}^n$, $\mathbf{V}^n$, $\boldsymbol{\omega}^n$, $\mathbf{x}_1^n$ and $\mathbf{x}_2^n$ *being known, we compute* $\mathbf{u}^{n+1/5}$, $p^{n+1/5}$ *via the solution of*

$$\begin{cases} \rho_f \displaystyle\int_\Omega \frac{\mathbf{u}^{n+1/5} - \mathbf{u}^n}{\triangle t} \cdot \mathbf{v} d\mathbf{x} - \int_\Omega p^{n+1/5} \boldsymbol{\nabla} \cdot \mathbf{v} d\mathbf{x} = 0,\ \forall \mathbf{v} \in \mathbf{W}_{0h}, \\ \displaystyle\int_\Omega q \boldsymbol{\nabla} \cdot \mathbf{u}^{n+1/5} d\mathbf{x} = 0,\ \forall q \in L^2_h, \\ \mathbf{u}^{n+1/5} \in \mathbf{W}_h,\ \mathbf{u}^{n+1/5} = \mathbf{g}_{0h}^{n+1} \text{ on } \Gamma,\ p^{n+1/5} \in L^2_{0h}. \end{cases} \tag{3.15}$$

Next, compute $\mathbf{u}^{n+2/5}$ *via the solution of*

$$\begin{cases} \displaystyle\int_\Omega \frac{\partial \mathbf{u}}{\partial t}\cdot \mathbf{v}d\mathbf{x} + \int_\Omega (\mathbf{u}^{n+1/5}\cdot\boldsymbol{\nabla})\mathbf{u}\cdot\mathbf{v}d\mathbf{x} = 0, \\ \forall \mathbf{v}\in \mathbf{W}_{0h}^{n+1,-},\ a.e.\ on\ (t^n,\ t^{n+1}), \\ \mathbf{u}(t^n) = \mathbf{u}^{n+1/5}, \\ \mathbf{u}(t)\in \mathbf{W}_h,\ \mathbf{u}(t) = \mathbf{g}_{0h}^{n+1}\ on\ \Gamma_-^{n+1}\times(t^n,\ t^{n+1}), \end{cases} \tag{3.16}$$

and set $\mathbf{u}^{n+2/5} = \mathbf{u}(t^{n+1})$.

Then, compute $\mathbf{u}^{n+3/5}$ *via the solution of*

$$\begin{cases} \rho_f\displaystyle\int_\Omega \frac{\mathbf{u}^{n+3/5}-\mathbf{u}^{n+2/5}}{\triangle t}\cdot\mathbf{v}d\mathbf{x} + \alpha\nu_f\int_\Omega \boldsymbol{\nabla}\mathbf{u}^{n+3/5}:\boldsymbol{\nabla}\mathbf{v}d\mathbf{x} = \rho_f\int_\Omega \mathbf{g}\cdot\mathbf{v}d\mathbf{x}, \\ \forall \mathbf{v}\in \mathbf{W}_{0h};\ \mathbf{u}^{n+3/5}\in\mathbf{W}_h,\ \mathbf{u}^{n+3/5} = \mathbf{g}_{0h}^{n+1}\ on\ \Gamma. \end{cases} \tag{3.17}$$

Now predict the motion of the center of mass and the angular velocity of the particle via

$$\frac{d\mathbf{G}}{dt} = \mathbf{V}(t), \tag{3.18}$$

$$\frac{d\mathbf{x}_i}{dt} = \mathbf{V}(t) + \boldsymbol{\omega}(t)\times\overrightarrow{\mathbf{G}(t)\mathbf{x}_i},\ for\ i=1,2, \tag{3.19}$$

$$(1-\rho_f/\rho_s)M_p\frac{d\mathbf{V}}{dt} = (1-\rho_f/\rho_s)M_p\mathbf{g} + \mathbf{F}_r, \tag{3.20}$$

$$(1-\rho_f/\rho_s)\frac{d(\mathbf{I}_p\,\boldsymbol{\omega})}{dt} = \overrightarrow{\mathbf{G}\mathbf{x}_r}\times\mathbf{F}_r, \tag{3.21}$$

$$\mathbf{G}(t^n) = \mathbf{G}^n,\ \mathbf{V}(t^n) = \mathbf{V}^n,\ (\mathbf{I}_p\,\boldsymbol{\omega})^n = (\mathbf{I}_p\,\boldsymbol{\omega})(t^n), \tag{3.22}$$

$$\mathbf{x}_1(t^n) = \mathbf{x}_1^n,\ \mathbf{x}_2(t^n) = \mathbf{x}_2^n,$$

for $t^n < t < t^{n+1}$. *Then set* $\mathbf{G}^{n+4/5} = \mathbf{G}(t^{n+1})$, $\mathbf{V}^{n+4/5} = \mathbf{V}(t^{n+1})$, $(\mathbf{I}_p\,\boldsymbol{\omega})^{n+4/5} = (\mathbf{I}_p\,\boldsymbol{\omega})(t^{n+1})$, $\mathbf{x}_1^{n+4/5} = \mathbf{x}_1(t^{n+1})$, $\mathbf{x}_2^{n+4/5} = \mathbf{x}_2(t^{n+1})$, *and* $\mathbf{u}^{n+4/5} = \mathbf{u}^{n+3/5}$.
With the center $\mathbf{G}^{n+4/5}$, $\mathbf{x}_1^{n+4/5}$ *and* $\mathbf{x}_2^{n+4/5}$ *obtained at the above step, we enforce the rigid body motion in the region* $B(t^{n+4/5})$ *occupied by the particle*

$$\begin{cases} \rho_f\displaystyle\int_\Omega \frac{\mathbf{u}^{n+1}-\mathbf{u}^{n+4/5}}{\triangle t}\cdot\mathbf{v}\,d\mathbf{x} + \beta\nu_f\int_\Omega \boldsymbol{\nabla}\mathbf{u}^{n+1}:\boldsymbol{\nabla}\mathbf{v}\,d\mathbf{x} \\ +(1-\dfrac{\rho_f}{\rho_s})M_p\dfrac{\mathbf{V}^{n+1}-\mathbf{V}^{n+4/5}}{\triangle t}\cdot\mathbf{Y} + (1-\dfrac{\rho_f}{\rho_s})\dfrac{(\mathbf{I}_p\,\boldsymbol{\omega})^{n+1}-(\mathbf{I}_p\,\boldsymbol{\omega})^{n+4/5}}{\triangle t}\cdot\boldsymbol{\theta} \\ =<\boldsymbol{\lambda}^{n+4/5},\ \mathbf{v}-\mathbf{Y}-\boldsymbol{\theta}\times\overrightarrow{\mathbf{G}^{n+4/5}\mathbf{x}}>_h,\ \forall\mathbf{v}\in\mathbf{W}_{0h},\mathbf{Y}\in\mathbb{R}^3,\ \boldsymbol{\theta}\in\mathbb{R}^3, \\ \mathbf{u}^{n+1}\in\mathbf{W}_h,\mathbf{u}^{n+1} = \mathbf{g}_{0h}^{n+1}\ on\ \Gamma,\ \boldsymbol{\lambda}^{n+4/5}\in\Lambda_h^{n+4/5},\mathbf{V}^{n+1}\in\mathbb{R}^3,\boldsymbol{\omega}^{n+1}\in\mathbb{R}^3, \end{cases} \tag{3.23}$$

$$<\boldsymbol{\mu},\ \mathbf{u}^{n+1}-\mathbf{V}^{n+1}-\boldsymbol{\omega}^{n+1}\times\overrightarrow{\mathbf{G}^{n+4/5}\mathbf{x}}>_h = 0,\ \forall\boldsymbol{\mu}\in\Lambda_h^{n+4/5}. \tag{3.24}$$

In (3.14)–(3.24), $\Gamma_-^{n+1} = \{\mathbf{x}|\mathbf{x}\in\Gamma,\ \mathbf{g}_{0h}^{n+1}(\mathbf{x})\cdot\mathbf{n}(\mathbf{x}) < 0\}$ and $\mathbf{W}_{0h}^{n+1,-} = \{\mathbf{v}|\mathbf{v}\in\mathbf{W}_h,\ \mathbf{v} = \mathbf{0}\ on\ \Gamma_-^{n+1}\}$, $\Lambda_h^{n+s} = \Lambda_h(t^{n+s})$, and $\alpha+\beta = 1$. In the numerical simulation, we usually choose $\alpha = 1$ and $\beta = 0$.

3.2. On the solution of subproblems (3.15), (3.16), (3.17), (3.18)-(3.22), and (3.23)-(3.24). The degenerated quasi-Stokes problem (3.15) is solved by an Uzawa/preconditioned conjugate gradient algorithm as in [11], where the discrete elliptic problems from the preconditioning are solved by a matrix-free fast solver from FISHPAK due to Adams et al. in [1]. The advection problem (3.16) for the velocity field is solved by a wave-like equation method as in [4, 5]. Problem (3.17) is a classical discrete elliptic problem which can be solved by the same matrix-free fast solver.

System (3.18)-(3.22) is a system of ordinary differential equations thanks to operator splitting. For its solution one can choose a time step smaller than $\triangle t$, (i.e., we can divide $\triangle t$ into smaller steps) to predict the translation velocity of the center of mass, the angular velocity of the particle, the position of the center of mass and the regions occupied by each particle so that the repulsion forces can be effective to prevent particle-particle and particle-wall overlapping. At each subcycling time step, keeping the distance as constant between the pair of points $\mathbf{x}_1$ and $\mathbf{x}_2$ in each particle is important since we are dealing with rigid particles. We have applied the following approach to satisfy the above constraint:

- Translate $\mathbf{x}_1$ and $\mathbf{x}_2$ according to the new position of the mass center at each subcycling time step.

- Rotate $\mathbf{Gx}_1$ and $\mathbf{Gx}_2$, the relative positions of $\mathbf{x}_1$ and $\mathbf{x}_2$ to the center of mass $\mathbf{G}$, by the following Crank-Nicolson scheme (a Runge-Kutta scheme of order 2, in fact):

$$\frac{\mathbf{Gx}_i^{new} - \mathbf{Gx}_i^{old}}{\tau} = \boldsymbol{\omega} \times \frac{\mathbf{Gx}_i^{new} + \mathbf{Gx}_i^{old}}{2} \tag{3.25}$$

  for $i = 1, 2$ with τ as a subcycling time step. By (3.25), we have $|\mathbf{Gx}_i^{new}|^2 = |\mathbf{Gx}_i^{old}|^2$ for $i = 1, 2$ and $|\mathbf{Gx}_2^{new} - \mathbf{Gx}_1^{new}|^2 = |\mathbf{Gx}_2^{old} - \mathbf{Gx}_1^{old}|^2$ (i.e., scheme (3.25) is distance and in fact shape preserving).

Remark 3.1 *In order to activate the short range repulsion force, we have to find the shortest distance between two ellipsoids. Unlike the cases for spheres, it is not trivial to locate the point from each surface of the ellipsoid where the distance is the shortest between two ellipsoids. There is no explicit formula for such distance. In practice, we first choose a set of points from the surface of each ellipsoid. Then we find the point among the chosen points from each surface at which the distance is the shortest We repeat this (kinf of relaxation) process in the neighborhood of the newly located point on each surface of ellipsoid untill convergence, usually obtained in very few iterations.*

For the shortest distance between the wall and ellipsoid, there exists an explicit formula. To check whether two ellipsoids overlap each other, there exists an algorithm used by people working on computer graphics and in robotics (e.g., see, [20]).

After solving (3.18)-(3.22), the rigid body motion is enforced in $B(t^{n+4/5})$, via equation (3.24). At the same time those hydrodynamical forces acting on the particles are also taken into account in order to update the translation and angular velocities of the particles. To solve (3.23)-(3.24), we use a conjugate gradient algorithm as discussed in [7]. Since we take $\beta = 0$ in (3.23) for the simulation, we actually do not need to solve any non-trivial linear systems for the velocity field; this saves a lot of

computing time. To get the angular velocity $\boldsymbol{\omega}^{n+1}$, computed via

$$\boldsymbol{\omega}^{n+1} = (\mathbf{I}_p^{n+4/5})^{-1}(\mathbf{I}_p\,\boldsymbol{\omega})^{n+1}, \tag{3.26}$$

we need to have $\mathbf{I}_p^{n+4/5}$, the inertia of the particle $B(t^{n+4/5})$. We first compute the inertia $\mathbf{I}_0$ in the coordinate system attached to the particle. Then via the center of mass $\mathbf{G}^{n+4/5}$ and points $\mathbf{x}_1^{n+4/5}$ and $\mathbf{x}_2^{n+4/5}$, we have the rotation transformation $\mathbf{Q}$ ($\mathbf{Q}\mathbf{Q}^T = \mathbf{Q}^T\mathbf{Q} = \mathbf{I}_d$, det$\mathbf{Q}$=1) which transforms vectors expressed in the particle frame to vectors in the flow domain coordinate system and $\mathbf{I}_p^{n+s} = \mathbf{Q}\mathbf{I}_0\mathbf{Q}^T$. Actually in order to update matrix $\mathbf{Q}$ we can also use *quaternion* techniques, as shown, in the review paper [3].

4. Numerical experiments.

4.1. One settling ellipsoid. The orientation of symmetric long body (loosely, a long body is a body where one dimension is much prevailing upon the other two) in liquids of different nature is a fundamental issue in many problems of practical interest (see [15], and references therein). In the first test case, we consider the simulation of the motion of a settling ellipsoid in a narrow channel of infinite length filled with a Newtonian fluid. The computational domain is $\Omega = (0,1) \times (0,0.25) \times (0,4)$ initially, then it moves down with the center of the ellipsoid (see, e.g., [13] for adjusting the computational domain according to the position of the particle). The fluid density is $\rho_f = 1$ and the fluid viscosity is $\nu_f = 0.01$. The flow field initial condition is $\mathbf{u} = \mathbf{0}$. The three semi-axes of the ellipsoid are 0.2, 0.1 and 0.1. The initial velocity and angular velocity of the ellipsoid are $\mathbf{0}$. The density of the ellipsoid is $\rho_s = 1.25$. Its vertical axis is the longest semi-axis (see Figure 4.1). The mesh size for the velocity field (resp., pressure) is $h_v = 1/80$ (resp., $h_p = 2h_v$). The time step is $\triangle t = 0.001$. The positions of the ellipsoid at different times in the channel are shown in Figure 4.1. (The computation was performed in a moving frame of reference, so the ellipsoid appears not moving downward.) The motion of the ellipsoid is very violent at the beginning, it moves very close to the side wall after release from its initial position. Later on the motion becomes periodic (see Figures 4.1 and 4.2). As expected, the ellipsoid turns its broadside to the stream while oscillating as shown in the last three snapshots of Figure 4.1. The averaged particle speed at the end of the simulation is about 4.256 so the particle Reynolds number with the long axis as characteristic length is 170.24.

4.2. Two ellipsoids sedimenting side-by-side. It had been observed experimentally by Joseph and Bai that when two ellipsoid-like long bodies sedimente side-by-side in a narrow channel filled with a Newtonian fluid, they interact each other periodically as shown in Figures 4.3. The particle Reynolds number is about 120. To reproduce this phenomenon, we consider the following test case. The computational domain is $\Omega = (0,1) \times (0,0.25) \times (0,4)$ initially, then it moves down with the lower center of two ellipsoids. The initial positions of the centers are $(0.22, 0.125, 0.75)$ and $(0.78, 0.125, 0.75)$, respectively. The frames rigidly attached to the ellipsoids initially are $\{(\cos\pi/3, 0, \sin\pi/3)$, $(0,1,0)$, $(\cos 5\pi/6, 0, \sin 5\pi/6)\}$ and $\{(\cos(-\pi/3), 0, \sin(-\pi/3))$, $(0,1,0)$, $(\cos\pi/6, 0, \sin\pi/6)\}$, respectively (see Figure 4.4). All others parameters are as in the previous case. Averaged terminal speed is about 2.497 obtained from last 300 time steps, so the averaged particle Reynolds number is 99.88 based on the length

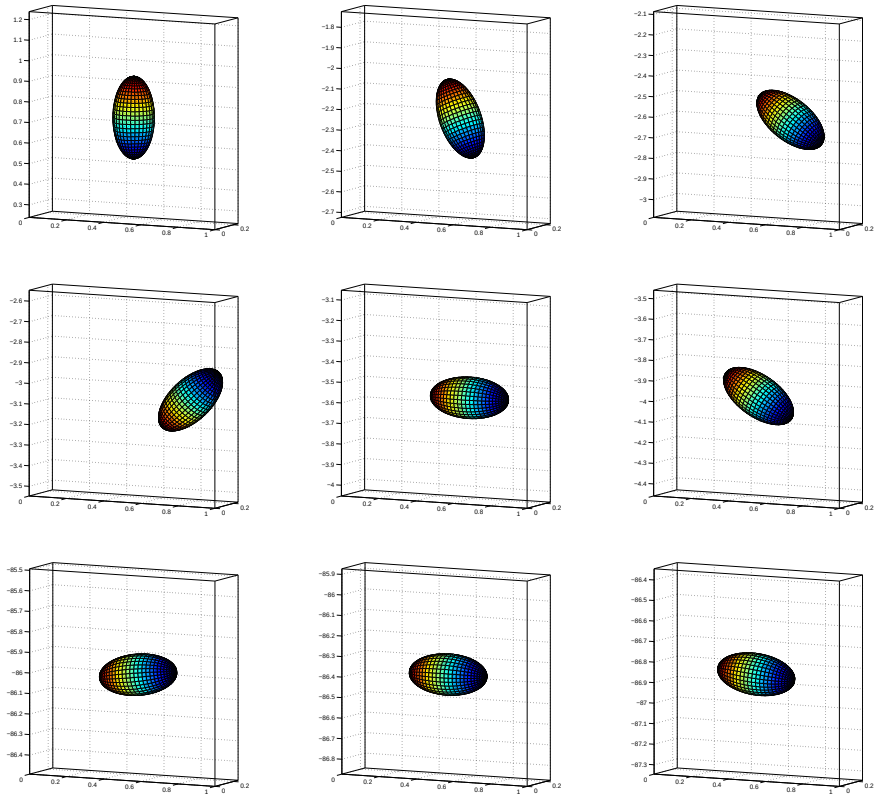

Figure 4.1: Position of the ellipsoid at $t = 0$, 0.41, 0.46, 0.56, 0.66, 0.75, 18.1, 18.18, and 18.28 (from left to right and from top to bottom).

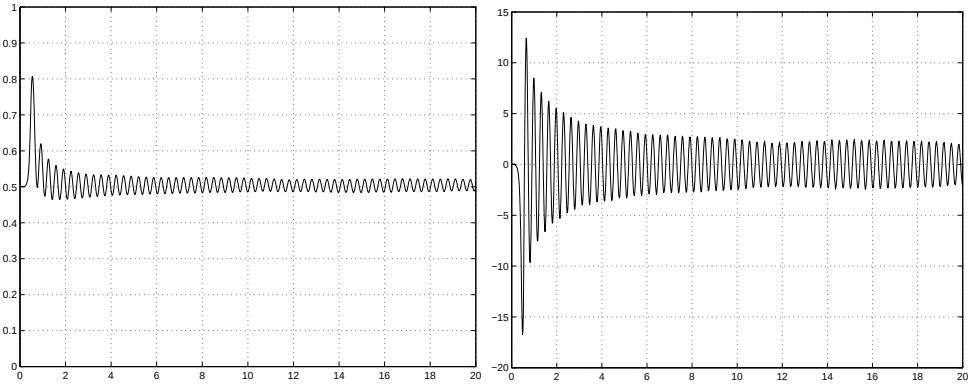

Figure 4.2: Histories of the x-coordinate of the center (left) and the y-component of the angular velocity of the ellipsoid (right) .

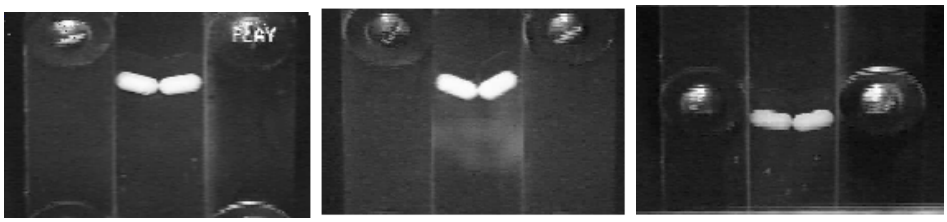

Figure 4.3: Snapshots of a period of the motion of two ellipsoid-like long bodies sedimenting in a narrow channel filled with a Newtonian fluid.

of the long axis (which is 0.4). In the simulation, we obtained result as seen in Figure 4.4 similar to the one in Figure 4.3 (the computation was performed in a moving frame of reference, so the ellipsoids appear not moving downward), which is in good agreement with experimental results qualitatively. In Figure 4.5, we can see very strong interaction between two ellipsoids of long axes 0.4. We also have tested the case with two ellipsoids of long axes 0.36 and found that they settle in the channel with very weak interaction between each other (see Figure 4.5).

Acknowledgments We acknowledge the helpful comments and suggestions of G.P. Galdi, J. He, and V.I. Paulsen. We acknowledge also the support of NSF (grants DMS-9973318, and CCR-9902035), Texas Board of Higher Education (ARP grant 003652-0383-1999), and DOE/LASCI (grant R71700K-292-000-99).

REFERENCES

[1] J. Adams, P. Swarztrauber, and R. Sweet. *FISHPAK: A package of Fortran subprograms for the solution of separable elliptic partial differential equations.* The National Center for Atmospheric Research, Boulder, CO, 1980.

[2] F. Baaijens. A fictitious domain/mortar element method for fluid-structure interaction. *Int. J. Numer. Meth. Fluids*, 35:743–761, 2001.

[3] J. C. K. Chou. Quaternion kinematic and dynamic differential equations. *IEEE transaction on robotics and automation*, 8:53–64, 1992.

[4] E. J. Dean and R. Glowinski. A wave equation approach to the numerical solution of the Navier-Stokes equations for incompressible viscous flow. *C.R. Acad. Sc. Paris*, 325(Serie 1):783–791, 1997.

[5] E. J. Dean, R. Glowinski, and T.-W. Pan. A wave equation approach to the numerical simulation of incompressible viscous fluid flow modeled by the Navier-Stokes equations. In J. D. Santo, editor, *Mathematical and Numerical Aspects of Wave Propagation*, pages 65–74, Philadelphia, PA, 1998. SIAM.

[6] R. Glowinski, T. I. Hesla, D. D. Joseph, T. W. Pan, and J. Periaux. Distributed Lagrange multiplier methods for particulate flows. In M. Bristeau, G. Etgen, W. Fitzgibbon, J. Lions, J. Periaux, and M. Wheeler, editors, *Computational Science for the 21st Century*, pages 270–279, Chichester, 1997. Wiley.

[7] R. Glowinski, T. Pan, T. Hesla, and D. Joseph. A distributed Lagrange multiplier/fictitious domain method for particulate flow. *International Journal of Multiphase Flow*, 25:755–794, 1999.

[8] R. Glowinski, T. W. Pan, T. I. Hesla, D. D. Joseph, and J. Periaux. A fictitious domain method with distributed Lagrange multipliers for the numerical simulation of particulate flow. In

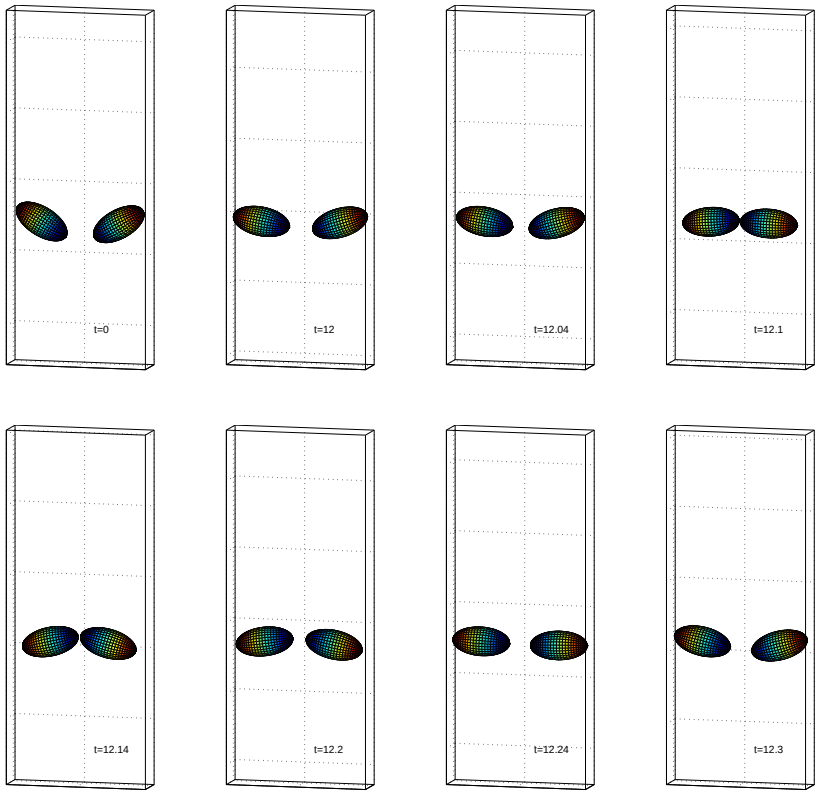

Figure 4.4: Position of ellipsoids at $t = 0$, 12, 12.04, 12.1, 12.14 12.2, 12.24, and 12.3 (from left to right and from top to bottom).

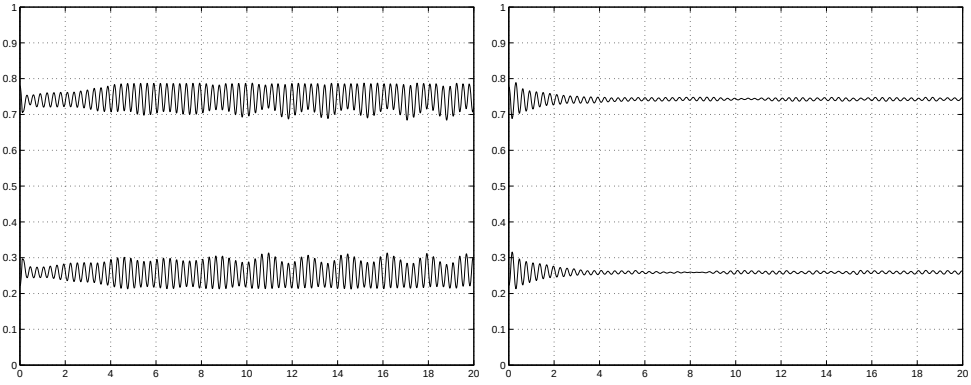

Figure 4.5: Histories of the x-coordinates of the centers of two ellipsoids of long axes 0.4 (left) and the x-coordinates of the centers of two ellipsoids of long axes 0.36 (right).

J. Mandel, C. Farhat, , and X. Cai, editors, *Domain Decomposition Methods 10*, pages 121–137, Providence, RI, 1998. AMS.

[9] R. Glowinski, T. W. Pan, T. I. Hesla, D. D. Joseph, and J. Periaux. A distributed Lagrange multiplier/fictitious domain method for flows around moving rigid bodies: Application to particulate flow. *Int. J. Numer. Meth. Fluids*, 30:1043–1066, 1999.

[10] R. Glowinski, T.-W. Pan, T. I. Hesla, D. D. Joseph, and J. Periaux. A fictitious domain approach to the direct numerical simulation of incompressible viscous flow past moving rigid bodies: Application to particulate flow. *J. Comput. Phys.*, 169:363–426, 2001.

[11] R. Glowinski, T.-W. Pan, and J. Periaux. Distributed lagrange multiplier methods for incompressible flow around moving rigid bodies. *Comput. Methods Appl. Mech. Engrg.*, 151:181–194, 1998.

[12] H. H. Hu. Direct simulation of flows of solid-liquid mixtures. *Int. J. Multiphase Flow*, 22:335–352, 1996.

[13] H. H. Hu, D. D. Joseph, and M. Crochet. Direct simulation of fluid particle motions. *Theoret. Comput. Fluid Dynamics*, 3:285–306, 1992.

[14] A. Johnson and T. Tezduyar. 3-d simulation of fluid-rigid body interactions with the number of rigid bodies reaching 100. *Comp. Meth. Appl. Mech. Eng.*, 145:301–321, 1997.

[15] Y. J. L. D. D. Joseph. Sedimentation of particles in polymer solutions. *J. Fluid Mech.*, 255:565–595, 1993.

[16] G. I. Marchuk. *Handbook of Numerical Analysis, Splitting and alternating direction methods*, volume I. Elsevier Science Publishers B.V., North-Holland, Amsterdam, 1990.

[17] B. Maury and R. Glowinski. Fluid-particle flow: a symmetric formulation. *C.R. Acad. Sc. Paris*, 324(Serie 1):1079–1084, 1997.

[18] C. S. Peskin. Numerical analysis of blood flow in the heart. *Journal of Computational Physics*, 25:220–252, 1977.

[19] C. S. Peskin and D. M. McQueen. Modeling prosthetic heart valves for numerical analysis of blood flow in the heart. *J. Comp. Phys.*, 37:113–132, 1980.

[20] E. Rimon and S. Boyd. Efficient distance computation using best ellipsoid fit. In *The IEEE International symposium on intelligent control, Glasgow, UK*, pages 360–365. IEEE, 1992.

[21] G. J. Wagner, N. Moes, W. K. Liu, and T. Belytschko. The extended finite element method for rigid particles in Stokes flow. *Int. J. Numer. Meth. Engng.*, 51:293–313, 2001.